Efficient coupling of a sub-5-nm-gap plasmonic crystal cavity with an integrated waveguide

Myung-Ki Kim[1,*]

[1]*Department of Physics, KAIST, Daejeon 305-701, South Korea*
[*]*kmk1852@kaist.ac.kr*

Abstract: An effective engineering method for efficient coupling between a tightly focused sub-5-nm-gap plasmonic crystal cavity and an integrated waveguide is proposed. A three-dimensionally tapered 2-nm-gap plasmonic crystal cavity exhibiting a mode volume of 6×10^{-6} $(\lambda/n)^3$ can efficiently couple to an integrated waveguide with over 90% efficiency by optimally selecting the number of air-holes in the plasmonic crystal. The field intensity is accordingly maximized, and its enhancement reaches to 205,000 for the light incident from the waveguide. Here, the optimal coupling is achieved by matching the radiation rate of the cavity mode to its absorption rate. In addition, the strongly enhanced field intensity boosts the spontaneous emission rate of the dipole emitter embedded in the cavity. The maximum radiative Purcell enhancement is calculated to be 362,000 where the quantum efficiency exceeds 50%.

References and links

1. M. T. Hill, Y.-S. Oei, B. Smalbrugge, Y. Zhu, T. de Vries, P. J. van Veldhoven, F. W. M. van Otten, T. J. Eijkemans, J. P. Turkiewicz, H. de Waardt, E. J. Geluk, S.-H. Kwon, Y.-H. Lee, R. Nötzel, and M. K. Smit, "Lasing in metallic-coated nanocavities," Nat. Photonics **1**(10), 589–594 (2007).
2. M. Khajavikhan, A. Simic, M. Katz, J. H. Lee, B. Slutsky, A. Mizrahi, V. Lomakin, and Y. Fainman, "Thresholdless nanoscale coaxial lasers," Nature **482**(7384), 204–207 (2012).
3. M. A. Noginov, G. Zhu, A. M. Belgrave, R. Bakker, V. M. Shalaev, E. E. Narimanov, S. Stout, E. Herz, T. Suteewong, and U. Wiesner, "Demonstration of a spaser-based nanolaser," Nature **460**(7259), 1110–1112 (2009).
4. R. F. Oulton, V. J. Sorger, T. Zentgraf, R.-M. Ma, C. Gladden, L. Dai, G. Bartal, and X. Zhang, "Plasmon lasers at deep subwavelength scale," Nature **461**(7264), 629–632 (2009).
5. M. P. Nezhad, A. Simic, O. Bondarenko, B. Slutsky, A. Mizrahi, L. Feng, V. Lomakin, and Y. Fainman, "Room temperature subwavelength metallo-dielectric lasers," Nat. Photonics **4**(6), 395–399 (2010).
6. C.-Y. Lu, S.-W. Chang, S. L. Chuang, T. D. Germann, and D. Bimberg, "Metal-cavity surface-emitting microlaser at room temperature," Appl. Phys. Lett. **96**(25), 251101 (2010).
7. S.-H. Kwon, J.-H. Kang, C. Seassal, S.-K. Kim, P. Regreny, Y.-H. Lee, C. M. Lieber, and H.-G. Park, "Subwavelength plasmonic lasing from a semiconductor nanodisk with silver nanopan cavity," Nano Lett. **10**(9), 3679–3683 (2010).
8. K. Okamoto, I. Niki, A. Shvartser, Y. Narukawa, T. Mukai, and A. Scherer, "Surface-plasmon-enhanced light emitters based on InGaN quantum wells," Nat. Mater. **3**(9), 601–605 (2004).
9. P. Neutens, P. Van Dorpe, I. De Vlaminck, L. Lagae, and G. Borghs, "Electrical detection of confined gap plasmons in metal–insulator–metal waveguides," Nat. Photonics **3**(5), 283–286 (2009).
10. W. Cai, J. S. White, and M. L. Brongersma, "Compact, high-speed and power-efficient electrooptic plasmonic modulators," Nano Lett. **9**(12), 4403–4411 (2009).
11. H. Xu, E. J. Bjerneld, M. Käll, and L. Börjesson, "Spectroscopy of single hemoglobin molecules by surface enhanced Raman scattering," Phys. Rev. Lett. **83**(21), 4357–4360 (1999).
12. H. G. Frey, S. Witt, K. Felderer, and R. Guckenberger, "High-resolution imaging of single fluorescent molecules with the optical near-field of a metal tip," Phys. Rev. Lett. **93**(20), 200801 (2004).
13. Z. Yuan, B. E. Kardynal, R. M. Stevenson, A. J. Shields, C. J. Lobo, K. Cooper, N. S. Beattie, D. A. Ritchie, and M. Pepper, "Electrically driven single-photon source," Science **295**(5552), 102–105 (2002).
14. A. V. Akimov, A. Mukherjee, C. L. Yu, D. E. Chang, A. S. Zibrov, P. R. Hemmer, H. Park, and M. D. Lukin, "Generation of single optical plasmons in metallic nanowires coupled to quantum dots," Nature **450**(7168), 402–406 (2007).
15. M.-K. Kim, Z. Li, K. Huang, R. Going, M. C. Wu, and H. Choo, "Engineering of metal-clad optical nanocavity to optimize coupling with integrated waveguides," Opt. Express **21**(22), 25796–25804 (2013).

16. M.-K. Kim, S. H. Lee, M. Choi, B.-H. Ahn, N. Park, Y.-H. Lee, and B. Min, "Low-loss surface-plasmonic nanobeam cavities," Opt. Express **18**(11), 11089–11096 (2010).
17. A. M. Lakhani, M. K. Kim, E. K. Lau, and M. C. Wu, "Plasmonic crystal defect nanolaser," Opt. Express **19**(19), 18237–18245 (2011).
18. X. Yang, A. Ishikawa, X. Yin, and X. Zhang, "Hybrid Photonic-Plasmonic Crystal Nanocavities," ACS Nano **5**(4), 2831–2838 (2011).
19. M. Davanco, Y. Urzhumov, and G. Shvets, "The complex Bloch bands of a 2D plasmonic crystal displaying isotropic negative refraction," Opt. Express **15**(15), 9681–9691 (2007).
20. T. Suzuki and N. Yamamoto, "Cathodoluminescent spectroscopic imaging of surface plasmon polaritons in a 1-dimensional plasmonic crystal," Opt. Express **17**(26), 23664–23671 (2009).
21. J. Conway, "Efficient Optical Coupling to the Nanoscale," PhD thesis, Univ. California (2006).
22. H. Choo, M.-K. Kim, M. Staffaroni, T. J. Seok, J. Bokor, S. Cabrini, P. J. Schuck, M. C. Wu, and E. Yablonovitch, "Nanofocusing in a metal–insulator–metal gap plasmon waveguide with a three-dimensional linear taper," Nat. Photonics **6**(12), 838–844 (2012).
23. K. Vahala, O. Microcavities; World Scientific Publishing Co, Hackensack, NJ (2004).
24. H. Haus, Waves and fields in optoelectronics; Prentice-Hall: Englewood Cliffs, NJ (1984).
25. E. M. Purcell, "Spontaneous emission probabilities at radio frequencies," Phys. Rev. **69**, 681 (1946).

1. Introduction

Recent advances in plasmonic cavities have provided a promising route to overcoming the diffraction limit of optical cavities by utilizing surface plasmon polaritons (SPPs), which enables us to confine electromagnetic energy within a sub-wavelength scale [1–7]. It has taken one step towards realizing various future optical devices, such as nano-scale high-speed optical emitters [8], detectors [9] and modulators [10], single-molecule spectroscopy [11], super-resolution optical imaging [12], and efficient single photon sources [13, 14]. However, their small feature sizes inevitably cause several significant issues such as inefficient coupling with waveguides and difficulty in fine engineering of the cavity mode [15]. For the practical use of plasmonic cavities, one should find the effective ways for efficient coupling and engineering of sub-wavelength-scale SPPs. In recent, plasmonic crystals, formed by periodic metallic structures, have been studied as a possible solution to engineer sub-wavelength-scale SPPs and control both near- and far-field patterns of sub-wavelength plasmonic cavities [16–20].

In this work, I suggest the effective engineering method for efficient coupling of the three-dimensionally tapered sub-5-nm-gap plasmonic crystal cavity to an integrated waveguide. By optimally selecting the number of air-holes in the plasmonic crystal, a tapered 2-nm-gap plasmonic crystal cavity exhibiting a mode volume of 6×10^{-6} $(\lambda/n)^3$ can efficiently couple to an integrated waveguide with over 90% efficiency. At the optimal coupling condition, the field intensity in the cavity as well as the spontaneous emission rate of the dipole emitter embedded in the cavity are highly maximized with enhancement factors of 205,000 and 362,000, respectively. I believe the proposed plasmonic crystal cavities will be the powerful devices for the practical use of sub-wavelength-scale SPPs as providing their excellent engineering and coupling properties.

2. MIM plasmonic crystal sub-5-nm-gap cavity

The simple way to build the plasmonic crystals is to attach the metal layers on the surface of photonic crystals [16–18] or to directly modulate the geometry of metallic structures with etching or lift-off process [19, 20], in which their scales should be adjusted to operate the frequency of interest. Figure 1(a) schematically presents the proposed one-dimensional metal-insulator-metal (MIM) plasmonic crystal nanobeam structure, where 100-nm-thick *Ag* layers sandwich a *Si* photonic crystal nanobeam to form the MIM configuration. The periodic air-holes along the nanobeam direction (*x*-direction) are drilled vertically through the entire *Ag-Si-Ag* layers, and the height and width of *Si* are 200 nm and 240 nm, respectively. To generate the plasmonic bandgap near the optical communication frequency of 193 THz, the lattice constant (*a*) is chosen to be 240 nm. Especially, the asymmetric elliptical air-holes (*x*:*y* = 0.35*a*:0.70*w*) are employed to more widely open the plasmonic bandgap near the bandedge of $k_x a/2\pi = 0.5$ as more separating the energy levels of the 1st and 2nd TM-like plasmonic crystal guided modes (TM_{even1} and TM_{even2} bands in Fig. 1(b)) involved in bandgap formation.

As shown in the plasmonic crystal band structure of Fig. 1(b), the wide plasmonic bandgap is observed near the frequency of 200 THz, and its gap width ($\Delta\omega / \omega$) is 0.34. Here, the band structure is numerically calculated using the finite-difference time-domain (FDTD) method under the Bloch's periodic boundary conditions of a unit cell. Figure 1(c) shows the simulated E^2 distributions of the 1st and 2nd TM-like plasmonic guided modes (overlaid arrows indicate directions of electric fields). We can see here that both modes stem from the fundamental anti-symmetric MIM SPP guided mode [21], and their different energy fillings generate the plasmonic bandgap near the bandedge of the plasmonic crystal.
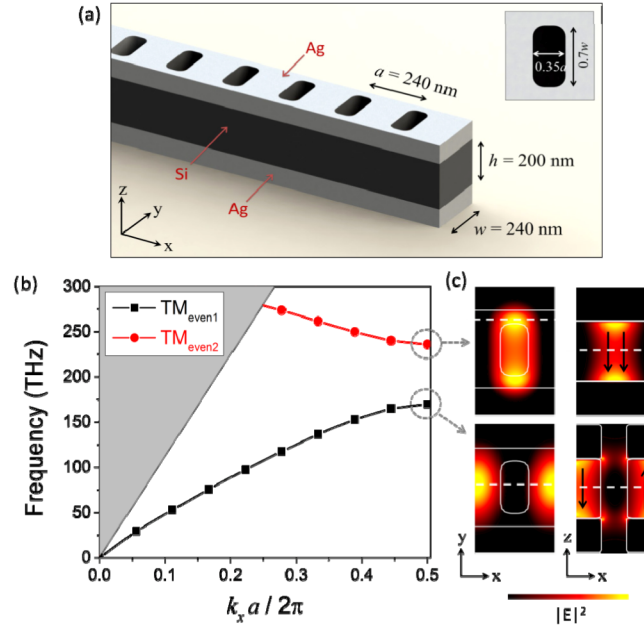

Fig. 1. (a) Schematic of proposed one-dimensional metal-insulator-metal (MIM; *Ag-Si-Ag*) nanobeam plasmonic crystal. (b) Calculated band structure of the MIM plasmonic crystal. (c) E^2 distributions of 1st and 2nd TM-like plasmonic bands at $k_x a/2\pi = 0.5$. Here, the arrows indicate the directions of electric field.

The plasmonic crystal cavity is formed by adding the defect (or by filling a couple of air-holes) in the middle of the plasmonic crystal, similarly to the formation of photonic crystal defect cavities [16, 17]. So, introducing the defect in the proposed MIM plasmonic crystal also creates the MIM SPP cavity mode in the region of the defect, and the resonant condition is determined by the length of the defect. Especially in the MIM cavity, the field can be more tightly confined into the extremely small space by tapering the cavity geometry, as shown in Fig. 2(a). Note that the MIM plasmonic crystal defect mode originates from the fundamental MIM SPP guided mode, and its energy density increases as reducing the gap size (or the gap area) normal to the propagating direction (*x*-direction) [21]. So, in the MIM tapered cavity, the energy density at the smallest gap is maximized compared to the other gaps, which leads to large reduction of the mode volume, because the mode volume is defined as the total cavity energy divided by the maximum energy density. Furthermore, the fundamental MIM SPP guided mode has no theoretical cutoff in size [22], so the mode volume of the tapered MIM cavity can be reduced without the limit of gap size. Among various possible taper geometries, the linear taper was introduced in the defect region, as shown in Fig. 2(a). The linear taper turned out to minimize losses generated in the taper section of the MIM SPP waveguide at the deep-subwavelength region [21], and recently three-dimensional MIM linear-taper structures were demonstrated [22]. As shown in Fig. 2(a), the width (*w*) and height (*h*) of *Si* are tapered down to w_{min} and h_{min}, respectively. Figure 2(b) shows the simulated E^2 distributions of the tapered MIM plasmonic crystal cavity, where *w* and *h* are 240 nm and 200 nm, respectively,

and the minimum width (w_{min}) and height (h_{min}) of Si are 5 nm. The cavity length (L in Fig. 2(b)) is chosen to be 750 nm, which tunes the resonant wavelength to 1550 nm. From this figure, we see that the electric field in the cavity is tightly confined in the region of the 5-nm gap, hugely reducing a mode volume (V_m) of the cavity. For $w_{min} = h_{min} = 5$ nm, V_m is calculated to be 8×10^{-5} $(\lambda/n)^3$ where λ and n are 1550 nm and 3.45, respectively. The quality factor is 100 that are almost limited by the absorption loss into the metal in the cavity.
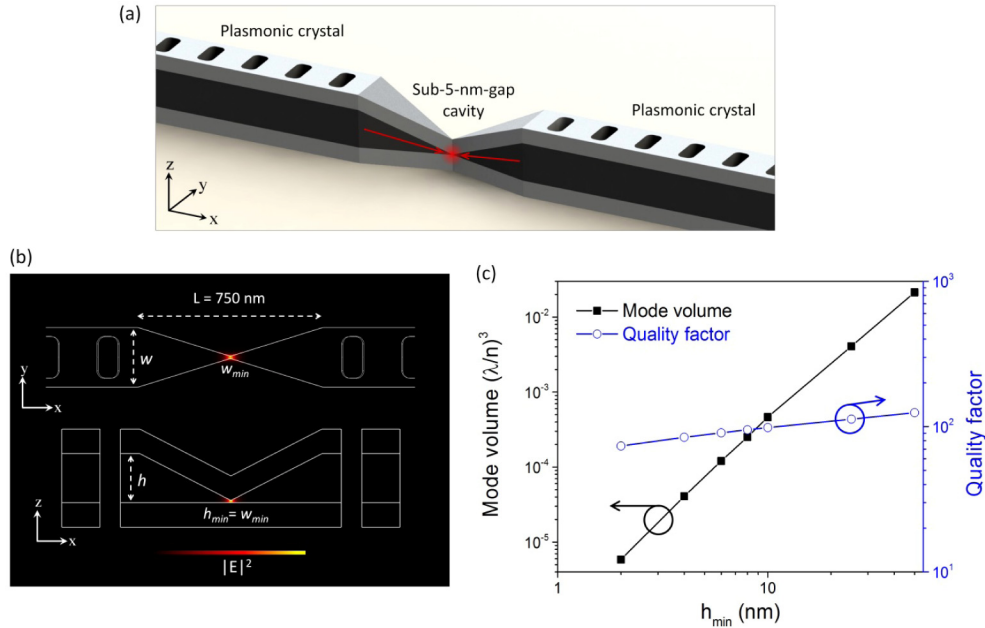

Fig. 2. (a) Schematic of three-dimensionally tapered plasmonic crystal cavity with a sub-5-nm central gap. (b) Simulated E^2 distributions of the cavity mode along xy- and xz-planes, where w and h of 240 nm and 200 nm are linearly tapered down to 5 nm ($w_{min} = h_{min} = 5$ nm), and the cavity length L is 750 nm. (c) Mode volume (V_m) and quality factor (Q) as a function of minimum height (h_{min}) of Si. The minimum width (w_{min}) of Si is equal to h_{min}.

In Fig. 2(c), the mode volume (V_m) and the quality factor (Q) as a function of a minimum gap size of the tapered plasmonic crystal cavity are investigated. In this calculation, I put w_{min} equal to h_{min}, so w and h are linearly tapered from 240 nm and 200 nm to the same size of h_{min}, respectively, at different rates. Figure 2(c) represents that V_m rapidly decreases as reducing h_{min}, while Q is not much influenced by h_{min}. If h_{min} is reduced from 50 nm to 2 nm (25-fold decrease), V_m decreases from 2×10^{-2} $(\lambda/n)^3$ to 6×10^{-6} $(\lambda/n)^3$ (3,300-fold decrease), but Q decreases only from 125 to 80 (1.6-fold decrease). It tells us that the field intensity in the tapered plasmonic crystal cavity can be highly enhanced as reducing the minimum gap sizes of h_{min} and w_{min}, because the field intensity in the cavity is proportional to the value of Q/V_m.

3. Efficient coupling to integrated waveguide

Since the MIM nanobeam structure itself with no air-holes can support the plasmonic waveguide mode propagating along the nanobeam direction, the direct and seamless integration of the MIM nanobem waveguide with the MIM plasmonic crystal cavity is allowed, as shown in Fig. 3(a). Furthermore, since both the cavity and waveguide modes stem from the fundamental MIM SPP guided mode, the coupling between those two modes is expected to be efficient due to the good mode matching. The coupling strength between the cavity and the waveguide is adjusted by selecting the number of air-holes (N in Fig. 3(a)) between them, because the plasmonic crystal with a small N acts as a partial Bragg mirror. In Fig. 3(b), the coupling efficiency and the quality factors as a function of N are investigated at

a fixed h_{min} of 2 nm. As reducing N, the coupling efficiency rapidly rises with increase of the radiation rate (or decrease of the radiation quality factor Q_{rad}) of the cavity mode. However, the absorption rate (or the absorption quality factor Q_{abs}) of the cavity mode is maintained almost constant. Here, Q_{rad} and Q_{abs} are calculated by comparing the radiation power and the metal-absorption power with the total power emitted from the cavity, respectively, using the relation of $Q^{-1} = Q_{rad}^{-1} + Q_{abs}^{-1}$. And, Q_{rad} consists of the cavity-to-air radiation (Q_{air}) and the cavity-to-waveguide radiation (Q_{guide}) with the relation of $Q_{rad}^{-1} = Q_{air}^{-1} + Q_{guide}^{-1}$, where Q_{air} and Q_{guide} are also calculated by comparing the cavity-to-air radiation power and the cavity-to-waveguide power with the total radiation power from the cavity, respectively. So, the coupling efficiency (η) is expressed as $\eta = Q_{guide}^{-1}/Q_{rad}^{-1}$. From Fig. 3(b), we note that the coupling efficiency exceeds 90% when N ≤ 2, and the radiation rate of the cavity mode becomes almost equal to its absorption rate ($Q_{rad} \sim Q_{abs} \sim 90$) when N = 2
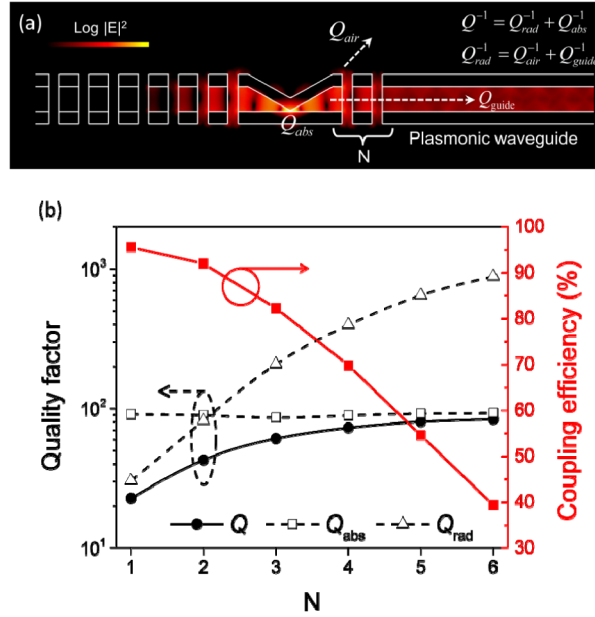

Fig. 3. (a) Simulated E^2 distribution of the three-dimensionally tapered plasmonic crystal cavity integrated with a plasmonic waveguide. Here, the number of air-holes (N) between the cavity and the waveguide controls the coupling strength. (b) Total quality factor (Q), radiation Q (Q_{rad}), absorption Q (Q_{abs}), and coupling efficiency as a function of N. Note that Q_{rad} becomes almost equal to Q_{abs} when N = 2.

4. Maximizing field intensity and spontaneous emission rate

Under the critical coupling condition in the waveguide-coupled cavity system, the energy (or the field intensity) inside the cavity is maximized for the light incident from the waveguide [23]. So, if the waveguide-coupled sub-5-nm-gap plasmonic crystal cavity in Fig. 3 satisfies the critical coupling condition, the field intensity in the cavity will be maximized. To find that condition, the coupled-mode equation describing a single cavity coupled with a one-port waveguide is established [24] as follows;

$$\frac{da}{dt} = j\omega_0 a - \frac{1}{2}(\gamma_{rad} + \gamma_{abs}) \cdot a + \sqrt{\eta \cdot \gamma_{rad}}\, s_+ \tag{1}$$

Here, ω_0 is the resonant frequency of the cavity mode, and γ_{rad} and γ_{abs} represent the radiation and absorption rates of the cavity mode having the relations of $\gamma_{rad} = \omega_0/Q_{rad}$ and $\gamma_{abs} = \omega_0/Q_{abs}$, respectively. The total electromagnetic energy in the cavity is given by $|a|^2$. The incident power from the waveguide is represented by $|S_+|^2$ in the last term, and η is the

coupling efficiency between the cavity and the waveguide. From Eq. (1), the total cavity energy in the steady state is given by

$$|a|^2 = \frac{4 \cdot \eta \cdot \gamma_{rad}}{(\gamma_{rad} + \gamma_{abs})^2} |s_+|^2 . \qquad (2)$$

By substituting $|a|^2$ and $|S_+|^2$ with $\varepsilon |E_{max}|^2 V_m$ and $\varepsilon |E_{input}|^2 A_{eff}(c/n_{eff})$, respectively, we can rewrite Eq. (2) as the intensity enhancement formula:

$$\frac{|E_{max}|^2}{|E_{input}|^2} = \frac{\eta \cdot \gamma_{rad}}{(\gamma_{rad} + \gamma_{abs})^2} \frac{4c}{n_{eff}} \frac{A_{eff}}{V_m} \qquad (3)$$

, where n_{eff} and A_{eff} are the effective refractive index and the effective mode area of the MIM plasmonic waveguide, respectively. This equation shows that the intensity enhancement is maximized when the condition of $\gamma_{rad} = \gamma_{abs}$ (or $Q_{rad} = Q_{abs}$) is satisfied. Note also that the enhancement is proportional to the coupling efficiency (η) and inversely proportional to the mode volume (V_m) of the cavity.
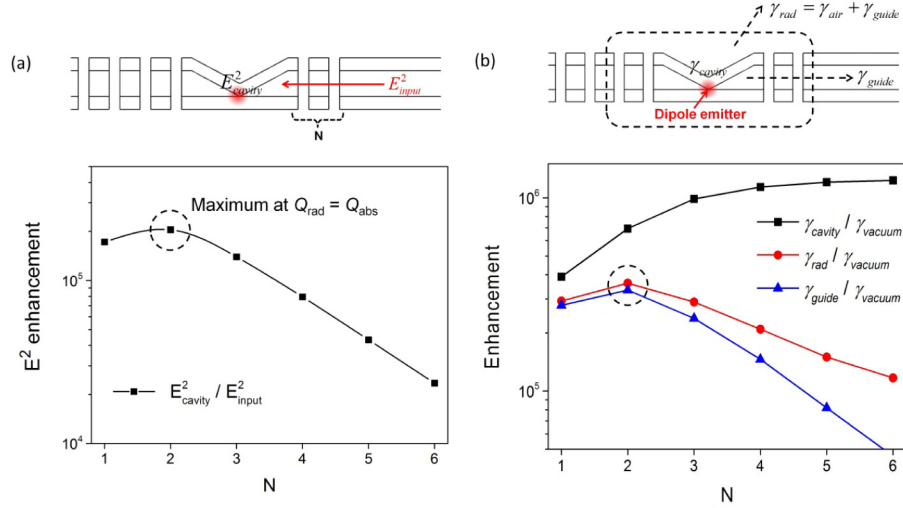

Fig. 4. (a) E^2 enhancement ($E_{cavity}^2 / E_{input}^2$) as a function of N. Here, the light is incident from the waveguide. (b) Enhancement factors of the spontaneous emission (SpE) rate of the dipole emitter embedded in the minimum gap of the cavity with different N. $\gamma_{cavity}/\gamma_{vaccum}$, $\gamma_{rad}/\gamma_{vaccum}$, and $\gamma_{guide}/\gamma_{vaccum}$ represent the enhancement factors of the cavity SpE rate, the radiative SpE rate, and the waveguide-coupled radiative SpE rate, respectively.

Figure 4(a) shows the simulated E^2 enhancement as a function of N when the light is incident from the waveguide. Here, h_{min} is fixed at 2 nm. As predicted in Eq. (3), the field intensity in the cavity is influenced by N (or γ_{rad}), and its enhancement is maximized at a certain optimal condition of N = 2 that is exactly equivalent to the predicted critical coupling condition of $\gamma_{rad} = \gamma_{abs}$ (or $Q_{rad} = Q_{abs}$), as shown in Fig. 3(b). At this optimal condition, the maximum E^2 enhancement is calculated to be 205,000. This large intensity enhancement is attributed to the extremely small mode volume (V_m), the high coupling efficiency (η), and the flexible engineering of the radiation rate (γ_{rad}) being able to satisfy the critical coupling condition ($\gamma_{rad} = \gamma_{abs}$). For reference, the E^2 enhancement for N = 0 is 18,300.

In addition to the field intensity enhancement, the small mode volume and the efficient coupling of the tapered plasmonic crystal cavity are also able to enhance the spontaneous emission rate of the dipole emitter embedded in the cavity. Figure 4(b) shows the enhancement factors of the spontaneous emission (SpE) rate of the dipole emitter as a

function of N, which are calculated by comparing the enhanced SpE powers of the dipole emitter with the SpE power in the vacuum state, using FDTD simulation. Here, the dipole emitter is located in the middle of the minimum gap at the center of the cavity. γ_{vaccum} in Fig. 4(b) is the SpE rate of the dipole emitter in free space with no optical structure. So, $\gamma_{cavity}/\gamma_{vaccum}$ represents the enhancement of the SpE rate influenced by the cavity mode, including the radiative and non-radiative emission rates. Its enhancement is theoretically proportional to Q/V_m of the cavity mode [25], so the gradual decrease of $\gamma_{cavity}/\gamma_{vaccum}$ as reducing N is explained by decrease of the total Q, as shown in Figs. 3(b) and 4(b). $\gamma_{rad}/\gamma_{vaccum}$ in Fig. 4(b) represents the enhancement of the radiative SpE rate, called Purcell enhancement (or radiative Purcell enhancement). It is influenced not only by the cavity Q/V_m but also by the quantum efficiency (QE) defined as

$$QE = \frac{\gamma_{rad}}{\gamma_{cavity}} = \frac{\gamma_{rad}}{\gamma_{rad} + \gamma_{abs}}. \tag{4}$$

So, $\gamma_{rad}/\gamma_{vaccum}$ is given by

$$\frac{\gamma_{rad}}{\gamma_{vacuum}} \propto \frac{Q}{V_m} \times \frac{\gamma_{rad}}{\gamma_{cavity}} \propto \frac{\gamma_{rad}}{\gamma_{cavity}^2} = \frac{\gamma_{rad}}{\left(\gamma_{rad} + \gamma_{abs}\right)^2}. \tag{5}$$

Equation (5) indicates that $\gamma_{rad}/\gamma_{vaccum}$ is maximized as satisfying the condition of $\gamma_{rad} = \gamma_{abs}$ (or $Q_{rad} = Q_{abs}$) that is exactly same with the critical coupling condition discussed in Eq. (3). Figure 4(b) clearly shows that $\gamma_{rad}/\gamma_{vaccum}$ is maximized at N = 2 as satisfying $Q_{rad} = Q_{abs}$. At this optimal condition, the Purcell enhancement is calculated to be 362,000 where QE is 52%. For reference, the Purcell enhancement for N = 0 is 17,100 where QE is 72%. $\gamma_{guide}/\gamma_{vaccum}$ in Fig. 4(b) represents the enhancement of the waveguide-coupled radiative SpE rate, expressed as multiplying $\gamma_{rad}/\gamma_{vaccum}$ by a coupling efficiency ($\eta = \gamma_{guide} / \gamma_{rad}$). As shown in Fig. 4(b), the values of $\gamma_{rad}/\gamma_{vaccum}$ and $\gamma_{guide}/\gamma_{vaccum}$ are being close as reducing N because of the increase of the coupling efficiency. At N = 2, the coupling efficiency is calculated to be 92% that is similar to the value shown in Fig. 3(b).
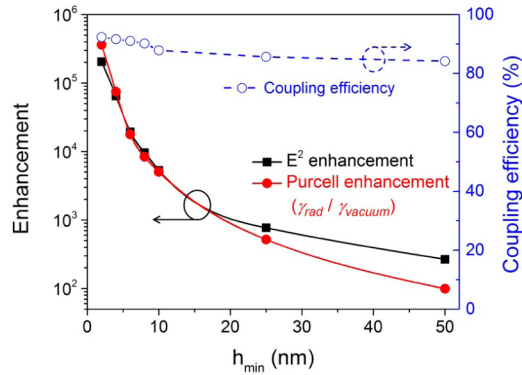

Fig. 5. E^2 and Purcell enhancements and coupling efficiency as a function of h_{min} at a fixed N of 2. Here, $w_{min} = h_{min}$.

Finally, the influences of h_{min} (= w_{min}) on the E^2 and Purcell enhancements and the coupling efficiency are investigated in Fig. 5. Since the E^2 and Purcell enhancements are inversely proportional to the mode volume of the cavity [Eq. (3) and Eq. (5)], the smaller h_{min} makes those enhancements much higher, as shown in this figure. When h_{min} is reduced from 50 nm to 2 nm at a fixed N of 2, the E^2 and Purcell enhancements increase from 270 to 205,000 (780-fold increase) and from 100 to 362,000 (3,620-fold increase), respectively. On the other hand, the coupling efficiency maintains almost high value from 84% to 92%. A

small decrease of the coupling efficiency for large h_{min} is due to the slight increase of the cavity-to-air radiation rate.

5. Summary

In summary, the effective engineering method to optimize coupling between a sub-5-nm-gap plasmonic crystal cavity and an integrated waveguide has been proposed. By optimally selecting the number of air-holes in the plasmonic crystal, a three-dimensionally tapered 2-nm-gap plasmonic crystal cavity exhibiting a mode volume of 6×10^{-6} $(\lambda/n)^3$ can efficiently couples to an integrated waveguide with over 90% efficiency. At the optimal coupling condition, the field intensity in the cavity as well as the spontaneous emission rate of the dipole emitter embedded in the cavity are highly maximized with enhancement factors of 205,000 and 362,000, respectively.

Acknowledgements